Biochemical and Biophysical Research Communications 391 (2010) 203–208

Contents lists available at ScienceDirect

Biochemical and Biophysical Research Communications

journal homepage: www.elsevier.com/locate/ybbrc

Structural and dynamic changes of the serum response element and the core domain of serum response factor induced by their association

Josef Štěpánek [a,b,c], Vladimír Kopecký Jr. [c], Alberto Mezzetti [a,d], Pierre-Yves Turpin [a], Denise Paulin [b], Bernard Alpert [b], Christian Zentz [a,*]

[a] Laboratoire Acides Nucléiques & Biophotonique, FRE CNRS 3207, Université Pierre et Marie Curie, 5 rue Henri Desbruères, 91030 Evry, France
[b] UR4, Université Pierre et Marie Curie, 7 quai St Bernard, 72252 Paris Cedex 5, France
[c] Institute of Physics, Faculty of Mathematics and Physics, Charles University in Prague, Ke Karlovu 5, 121 16 Prague 2, Czech Republic
[d] Laboratoire de Spectrochimie Infrarouge et Raman, UMR 8516, Université de Sciences et Technologies de Lille, Cité Scientifique, Villeneuve d'Ascq, France

ARTICLE INFO

Article history:
Received 25 October 2009
Available online 10 November 2009

Keywords:
Core-SRF
SRE
c-fos
Specific recognition
Raman spectroscopy

ABSTRACT

Transcriptional activity of serum response factor (SRF) is dependent on its binding to the CC(A/T)$_6$GG box (CArG box) of serum response element (SRE). By Raman spectroscopy, we carried out a comparative analysis, in solution, of the complexes obtained from the association of core-SRF with 20-mer SREs bearing wild-type and mutated c-fos CArG boxes. In case of association with the wild type c-fos CArG box, the complex does not bring out the expected Raman signature of a stable bending of the targeted SRE but keeps a bend–linear conformer oligonucleotide interconversion. The linear conformer population is larger than that of free oligonucleotide. In the core-SRF moiety of the wild-type complex a large spectral change associated with the CO-groups from Asp and/or Glu residues shows that their ionization states and the strength of their interactions decrease as compared to those of mutated non-specific complexes. Structural constraints evidenced on the free core-SRF are released in the wild-type complex and environmental heterogeneities appear in the vicinity of Tyr residues, due to higher water molecule access. The H-bonding configuration of one Tyr OH-group, in average, changes with a net transfer from H-bond acceptor character to a combined donor and acceptor character. A charge repartition distributed on both core-SRF and targeted SRE stabilizes the specific complex, allowing the two partners to experience a variety of conformations.

Introduction

Serum response factor (SRF) activates several muscles specific genes as well as genes that respond to mitogens [1–3]. The transcriptional activity of a number of these genes is associated with SRF binding to the so called CArG box sequence CC(A/T)$_6$GG [1–3]. The core domain of SRF (core-SRF) is competent to specifically bind to CArG boxes of serum response element (SRE) and recruit accessory transcription factors [4–6]. In the available X-ray structures of the core-SRF co-crystallized with SREs bearing transcriptional active CArG boxes of c-fos and α-actin genes, the functions of DNA binding, core-SRF homodimerization and accessory factor recruitment are integrated into a compact structural unit [6,7]. The SREs are bent around the protein by a ~72° overall angle. Biochemical studies are consistent with this conclusion finding from the crystallized complexes [8,9]. However, other MADS box proteins only minimally distort the DNA, despite strong sequence similarity with SRF and related DNA binding domains [9]. The degree of DNA bending is expected to play a role in the architecture of higher order transcription complexes. Nature of cellular processes including recombination, replication and gene regulation are thought to be linked to the degree of DNA bending in response to protein binding [10,11]. Thus, a direct correlation has been emphasized between the degree of oligonucleotide bending and the ability of core-SRF to recognize targeted CArG sequences [9]. However, the free SREs, in solution, are in a dynamic equilibrium between bent and linear conformers [12]. Thus, it is rightful to question the role played by this conformer interconversion in the adjustment of the specific core-SRF dimer on the c-fos CArG box? By which mechanism core-SRF recognizes its SRE target?

In order to unravel the interactions between core-SRF and the targeted 20-mer oligonucleotide (SRE^{fos}) we have employed Raman spectroscopy to study their complex in solution. The 20-mer SRE^{fos} reproduces the SRF recognition element of c-fos enhancer:

Abbreviations: Core-SRF, core domain of the serum response factor; SRE, oligonucleotide reproducing a serum response factor recognition element and/or its mutants

* Corresponding author. Fax: +33 169 874 360.
E-mail address: christian.zentz@upmc.fr (C. Zentz).

0006-291X/$ - see front matter © 2009 Elsevier Inc. All rights reserved.
doi:10.1016/j.bbrc.2009.11.032

5′-d(GGATGTC$_5$C$_4$A$_3$T$_2$A$_1$T$_{+1}$T$_{+2}$A$_{+3}$G$_{+4}$G$_{+5}$ACAT)3′ (c-fos CArG box numbered) [13]. A detailed Raman analysis on the core-SRF with SRE^{fos} was compared to the complexes of core-SRF with two mutants of the c-fos CArG box i.e. the single $C_5 \rightarrow G$ (SRE^{Gfos}) and the double $C_5C_4 \rightarrow GG$ (SRE^{GGfos}), which have been found to bind one and four core-SRF monomers on average, respectively [4].

Materials and methods

Protein. The present study utilizes the SRF fragment (residues 124–245, core-SRF) expressed and purified as described previously [4]: mrgshhhhhhgs$_{124}$GPVSGAVSGAKPGKKTRGRVKIKMEFIDNKLRR YTTFSKRKTGIMKKAYELSTLTGTQVLLLVASETGHVYTFATRKLQPMITS ETGKALIQTCLNSPDSPRSDPTTDQRMSATGFEETKLN$_{245}$ (lower case letters represent His-tag).

Oligonucleotides and their complexes. The 20-mer oligonucleotide SRE^{fos} and the two mutants including modifications at the end of the CArG box: the SRE^{Gfos} gCATATTAGG and the SRE^{GGfos} ggATATTAGG (mutations are indicated in lower case letters) were purchased from Masaryk University (Brno, Czech Republic). The duplexes were prepared as described elsewhere [12]. Core-SRF-SRE complexes were prepared by mixing 10 mL of 5×10^6 M of core-SRF with a concentrated solution of the oligonucleotide so as to get a concentration of 2.5×10^6 M SRE in a 10 mM Tris/HCl buffer, pH 8.5, 0.1 M NaCl, 1 mM dithiothreitol, 1 mM EDTA.

Raman spectroscopy. Samples, placed in a temperature-stabilized microcell of 12 μL volume, were kept at 10 °C and excited by the 488.0 nm Ar^+ laser. Raman spectra were recorded on a Jobin–Yvon T64000 CCD Raman spectrometer with about 4 cm^1 resolution. An accuracy of Raman shift was refined by using a neon glow-lamp spectrum recorded after every analyzed sample. Undesirable spectral contributions of water, Tris (represented by four spectral profiles obtained from Tris spectra measured at various pH and concentrations), urea, glass, and 6th degree polynomial background were subtracted using a least square fit. In the case of core-SRF–SRE complexes, primarily the fit was applied to a difference spectrum between the complex and its free components. Secondary the background corrected spectrum of the complex was determined. The fit provided concentration-dependent coefficients of core-SRF and SRE in the samples of complexes: SRE concentrations were computed by using as a reference the spectra of pure SRE duplexes at known concentrations. Core-SRF concentrations were estimated from the Raman intensity in the region of the Phe band ~1000 cm^1 by using a correlation between this Raman signature and the molar concentration obtained from a reference set of 7 proteins. The estimated concentration of free core-SRF was 5×10^5 M. In the mixed core-SRF and SRE solution the yield of concentrating procedure was substantially higher: the SRE concentration was about 2×10^4 M, and the core-SRF concentration was comparable with the highest core-SRF to SRE ratio in the case of the SRE^{fos} without mutation.

Protein secondary structure analysis. Estimation of the secondary structure content of the core-SRF was achieved by using the pattern recognition least-squares method (LSA) [14] and the reference intensity profiles (RIP) method [15] (implemented as Matlab™ routines in Vibrational Spectroscopy Toolbox and Applications [16]) in the region of amide I. We have tested impacts of the weak extraneous bands subtraction of the solvent spectrum inclusion as an additional spectral profile and/or of the Raman spectrum smoothing with following findings: the subtraction of the side bands at 1606 and 1615 cm^{-1} caused negligible differences in the estimation for RIP method. Noticeable improvement was obtained for the LSA. The subtraction of solvent spectrum slightly improved results of the RIP whereas smoothing had no significant impact on any method.

Results and discussion

SRE^{fos}, SRE^{Gfos} and SRE^{GGfos} moieties reshaping upon complex formation with core-SRF

SRE^{fos} spectral features

Fig. 1 shows the Raman spectrum of the complex [(core-SRF-homodimer)–SRE^{fos}] and the difference between this spectrum and the sum of the free constituents, core-SRF (Fig. 4) and SRE^{fos} alone, whose Raman spectrum is identical with that previously displayed [12]. The difference spectrum reflects the changes undergone by both partners upon complex formation. Several spectral features arise from changes in the furanose ring puckering: Peak/trough pairs at 724/730 and 740/758 cm^1, resulting from a downshift of the 729 (dA) and 749 cm^{-1} (dT) bands, and trough at 1345 cm^1, from (dA), resulting from a shift and an intensity decrease of the band at 1340 cm^1; these spectral features are consistent with a net change in dT and dA furanose conformations from the C2′endo/anti to C3′endo/anti [17,18]. The trough at 778 cm^1, probably resulting from a shift of the 784 cm^1 component of the 784/791 cm^1 doublet, expresses changes in the conformation of deoxycitidine and/or deoxythymidine [18]. The band at 1053 cm^1 and the trough at 1465 cm^1 imply altered backbone geometry [19]. The intensity decrease of the bands at 731 (dA), 758 (dT), 778 (dC, dT), 1018 (dG, dT), 1143 (dT), 1305 (dA), 1345 (1340) (dA), 1377 (dT), 1490 (dG), 1580 (1577) cm^1 (dA) results from a more effective base stacking affecting adenine and thymine, and also guanine [12]. The trough at 1018 cm^1 originates in an up shift of the 1013 cm^1 band, and may reflect different H-bonding environment of guanine and/or thymine [20]. The broad band at 1252 cm^1 partly results from shifts of the 1256 cm^{-1} band and expresses a wide rehandling of H-bonds at thymine base sites [17]. These changes show a redistribution of water molecules originating from the (A/T) domain of the CArG box.

On the whole, this Raman profile suggests a global structure change, inside B-DNA family, of the SRE^{fos} moiety [12]. Indeed, this structural adjustment is not limited to the central (A/T) domain of the CArG box but includes the bordering G bases because guanine signal (1490 cm^1) is also affected [21]. The changes induced in the spectrum of SRE^{fos} by the assembling of the specific complex are similar to those resulting from a larger population of linear conformers [12]. Thus, the equilibrium between bend and linear conformers of SRE^{fos} moiety is shifted toward the linear conformer as compared to that of the free oligonucleotide. This shift is though not linked with a dehydration process. Probably, the broad band at 1252 cm^{-1} reflects a non homogeneous water molecule redistribution at thymine base sites, hence a polymorphism of the (A/T) domain of this complex [17].

SREG^{fos} and SRE^{GGfos} spectral features

The difference Raman spectra reflecting changes of both moieties upon core-SRF–SRE^{Gfos} and core-SRF–SRE^{GGfos} complex formation are presented in Figs. 2 and 3, respectively. Both spectra exhibit some similarities. The spectra of free oligonucleotides are identical with those previously displayed [12]. Spectral features common to SRE^{Gfos} and SRE^{GGfos} upon core-SRF binding involve changes in the sugar pucker: the peak/trough pair at 725/731 cm^{-1} expresses a downshift of the band at 729 cm^1 reflecting changes from C2′endo/anti toward C3′endo/anti for (dA). The bands at 1446 cm^{-1} (1449 in case of SRE^{GGfos}) and the trough at 925 (927, SRE^{GGfos}) cm^1 imply deoxyribose changes [18,19]. The intensity decrease of the bands at 731, 1143, 1346, 1380, 1493, 1582 cm^{-1} for SRE^{Gfos} and at 688, 731, 1019, 1305, 1381, 1488, 1580 cm^{-1} for SRE^{GGfos} results from a more effective base stacking affecting adenine and thymine, and also guanine. In the spectral

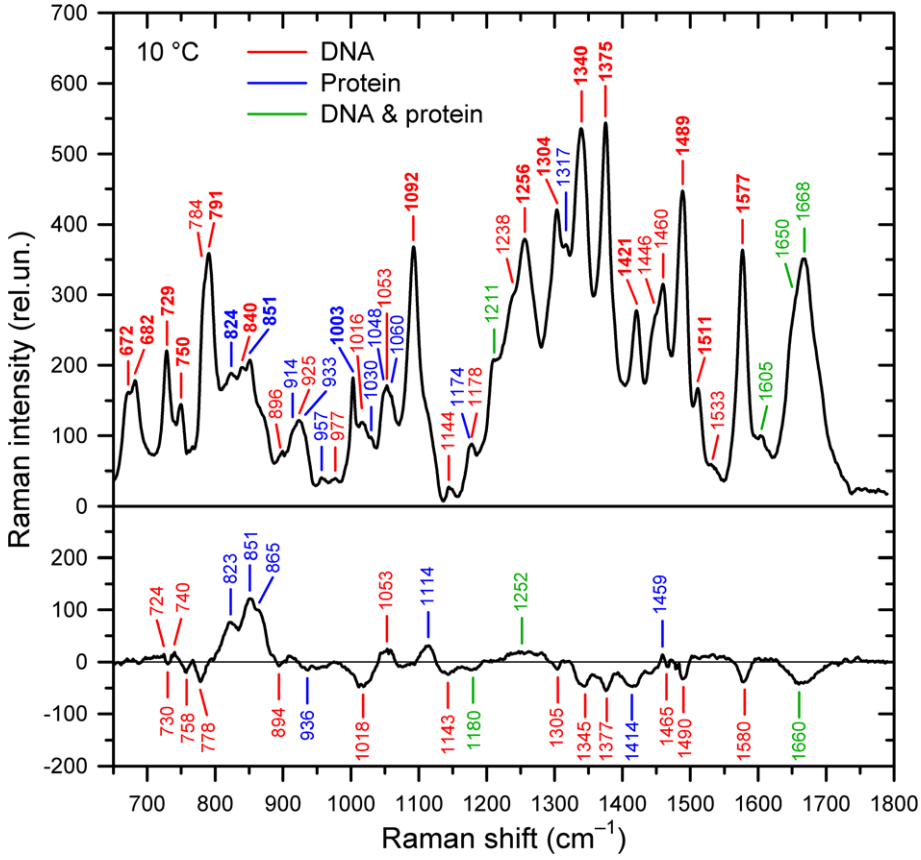

Fig. 1. Raman spectrum of the [(core-SRF-homodimer)–SRE^{fos}] complex (top) and its difference from a sum of free constituents, core-SRF monomer plus SRE^{fos} (bottom). Peak labels in black (red) color correspond to SRE part of the complex, in light gray (blue) to protein part and those in dark gray (green) are overlap of both. Numbers in bold face correspond to well resolved bands with precision of the peak position ±1 cm^{-1}, other have precision ±3 cm^{-1}. (For interpretation of colour mentioned in this figure, the reader is referred to the web version of this article.)

features particular to SRE^{Gfos}, a trough at 1346 cm^{-1} resulting from a shift of the 1340 cm^{-1} band, is a consequence of a change in the sugar pucker from C2′endo/anti to C3′endo/anti (dA) [17]; the peak/trough pair at 1485/1493 cm^{-1}, consequence of a downshift of the band at 1489 cm^{-1}, is associated with a redistribution of hydrogen bonds probably with guanine [21]. Some spectral features are characteristic of SRE^{GGfos}: namely negative band at 688 cm^{-1} and peak/trough pair at 1087/1098 cm^{-1} (PO_2^-) [18,19]. They correspond to perturbation of guanine bases and phosphate groups which bear large dipoles and charges [22]. Thus, this complex mainly involves electrostatic interactions. A weakening of H-bonds at adenine and thymine base sites probably is the consequence of a release of water molecules from the (A/T) domain of the CArG boxes of SRE^{Gfos} and SRE^{GGfos}: trough at 1380 cm^{-1}, band at 1508 cm^{1} and derivative feature with peak/trough pair at 1572(+)/1582(−) cm^{-1} evidence shifts of the bands at 1375 cm^{-1} (dT), 1511 and 1577 cm^{-1} (dA), respectively, for SRE^{Gfos}: band at 1249, 1507 and troughs at 1381, 1580 cm^{1}, are consequence of shifts of the bands at 1256, 1375 cm^{1} (dT), 1511 and 1577 cm^{1} (dA), respectively, for SRE^{GGfos} [17]. All things considered, there are striking similarities between the changes induced in the spectra of SRE^{Gfos} and SRE^{GGfos} by the binding of core-SRF. Both Raman signatures reflect an increase in the population of linear conformers with regard to free oligonucleotides.

Concluding remarks on SREs

The SRE^{fos} and its two mutants, upon complex formation with core-SRF, exhibit a larger population of linear conformers as compared with free oligonucleotides. We may conclude that the strains exerted by core-SRF on SREs retain conversion dynamics of the oligonucleotide moieties and change the frequency of the process. The bent angle of SRE^{fos} measured by crystallography or electrophoresis techniques may not represent a static bent, but the average between different states of DNA angles within the complexes with core-SRF. There are indications of a redistribution of the strains exerted on the free oligonucleotides by the binding interactions with core-SRF: a more effective base stacking and a more distinct presence of 3′endo conformation of furanose ring against a higher percentage of 2′endo/anti as compared with free SREs. Moreover, each SRE presents slightly different Raman signature, thus distinctive linear forms upon complex formation with core-SRF. These variations in the linear conformers originate in different mutual static and dynamic constraints exerted between the oligonucleotides and core-SRF.

Core-SRF alone and bound to SREs

Free core-SRF

Fig. 4 shows the Raman spectrum of free core-SRF in solution. Several peaks can be assigned to peptidyl backbone and amino acids residues (Table S1). Both amide I and amide III bands reveal a distribution of secondary structures. The asymmetrical amide I at 1667 cm^{-1}, correlated to the peak at 1245 cm^{-1} in amide III region are indicative of β-sheet structure; the peak at 1275 cm^{-1} in the amide III, the shoulder near 1650 cm^{-1} in the amide I band and the peak at 934 cm^{1} are indicative of α-helix structure [23,24]. Estimation of the secondary structure content of free core SRF was achieved by using LSA and RIP method in the region of amide

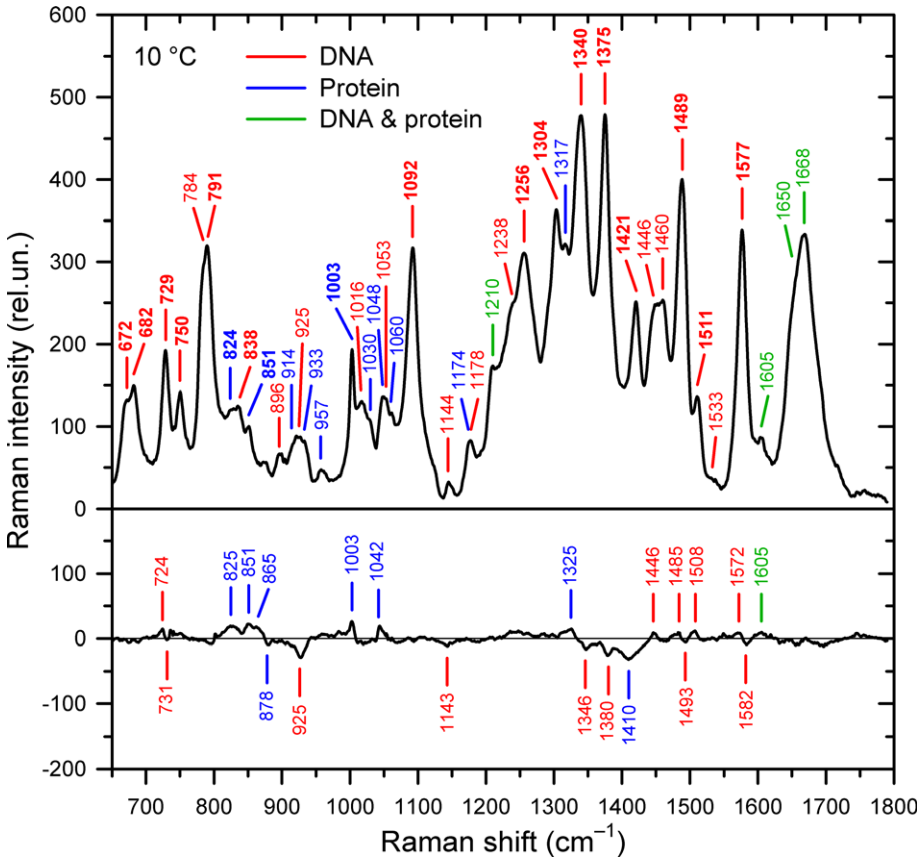

Fig. 2. Same as Fig. 1, but for core-SRF–SRE^{Gfos} complex.

I band [14–16]. Both approaches provided satisfactorily good fits and mutually consistent results which are summarized in Table S2. We have found 29–34% content of α-helix and 37–39% of β-sheets. Then free core-SRF in solution exhibits a secondary structure not very different from that found in crystallized complexes [6,7]. The tyrosine doublet consists of well resolved components at 825 and 853 cm^1. The I_{853}/I_{825} intensity ratio reflects the average hydrogen-bonding environment of the OH-groups of Tyr158, Tyr173 and Tyr195. Then, in the case of free core-SRF, it amounts to 2. The intensity ratio of a tyrosine doublet (I) is a diagnostic for the H-bond states of its OH-group [25]. If I = 2.5 the hydroxyl is acceptor of a strong hydrogen bond from a positive donor group as Lys and/or Arg residues and is denoted A state. If I = 1.25 the hydroxyl acts both as donor and acceptor of moderate H-bonds, as for those exposed to water molecules, and corresponds to a so called E state. The value of 2 of the Tyr intensity ratio of free core-SRF is consistent with the distribution 2A + 1E. The carboxyl groups of glutamic (6) and aspartic (3) acid residues probably contribute to the well resolved band at 1406 cm^{-1} [24].

Core-SRF moiety reshaping upon wild type specific complex formation with SRE^{fos}

The asymmetrical trough at 1660 cm^1, partly originating in the amide I, corresponds to a reduction of β-sheets content and, consistently with the trough at 936 cm^{-1}, of α-helix content [23,24]. The band at 865 and the trough at 936 cm^1 involve various CC stretching modes [26]. The broad trough at 1414 cm^1 originates in the 1406 cm^1 band and corresponds to a decrease in the ionization state of carboxyl groups with most probably a weakening of the interactions involving Glu and/or Asp [24]. Indeed Glu174 and Glu190 are involved in the core-SRF dimer interface and the side chain of Asp152 and Glu190 interacts with Arg157 [6]. The assembling of the core-SRF dimer on the SRE^{fos} and the repartition of the electrostatic charges of the protein moiety within the complex are deeply linked [27]. On the other hand, the tyrosine doublet intensity ratio (I_{851}/I_{823}) takes a value of 1.6. This value is consistent with a distribution of 1A + 2E. Thus, hydrogen bonds between one Tyr residue hydroxyl, in average, and most probably Arg and/or Lys residue(s) are weakened and this hydroxyl becomes more exposed to water molecules. The decrease of the Tyr doublet intensity ratio shows a redistribution in the hydrogen-bonding environment of the tyrosine hydroxyls [25]. Actually, a decrease in α-helix and β-sheet content of core-SRF moiety is consistent with a weakening of the H-bond network. The width of both doublet components is a consequence of a less homogeneous Tyr –OH group environments as compared to free core-SRF.

Comparison of core-SRF moiety in the wild type specific and mutated non-specific complexes

The decrease in the ionization states of carboxyl groups of core-SRF moieties affects stronger electrostatic interactions in case of SRE^{fos} (broad trough at 1414 cm^{-1} reflecting changes of the band at 1406 cm^1) than in case of SRE^{GGfos} and SRE^{Gfos} (troughs at 1410 cm^1) (Figs. 1–3). Thus, the specific core-SRF dimer bound to SRE^{fos} involves a more regular distribution of carboxyl group charge interactions. Then, the specific complex exhibits an electrostatic network more homogeneous than that of the non-specific associations most probably linked to a higher water molecule exposure. Whereas, the core-SRF polymerization process on SRE^{GGfos} could be due to a too high electrostatic effect. Indeed, electrostatic interactions are established between multiple core-SRF piled up and SRE^{GGfos}. On the other hand SRE^{Gfos} binding to

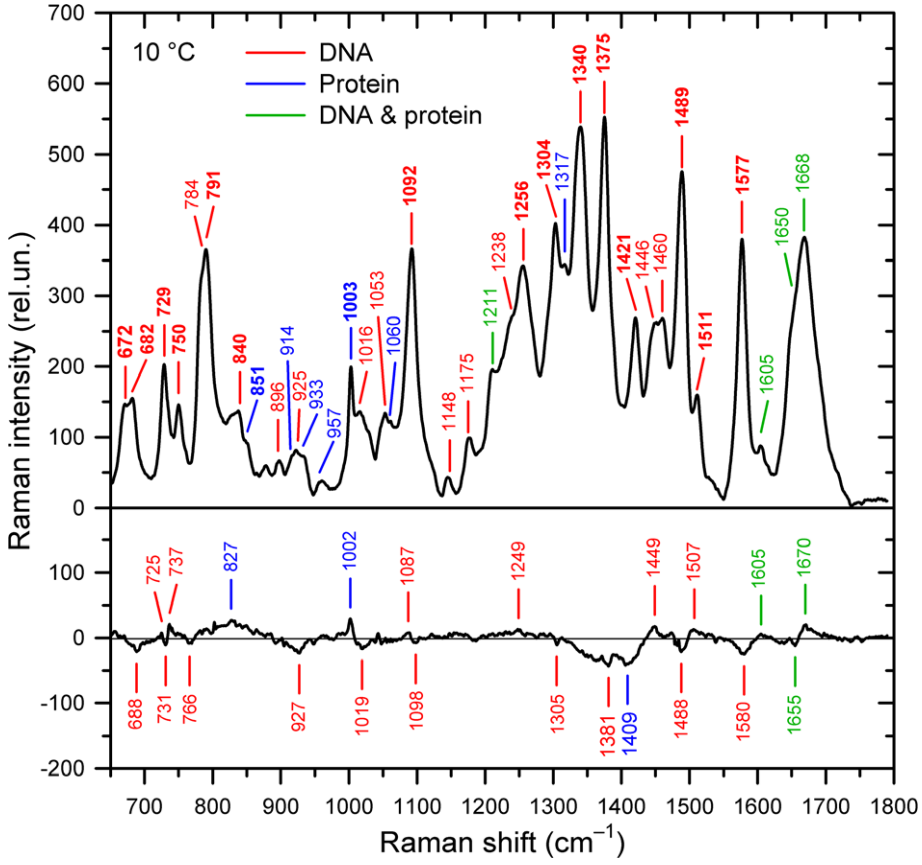

Fig. 3. Same as Fig. 1, but for core-SRF–SRE^{GGfos} complex.

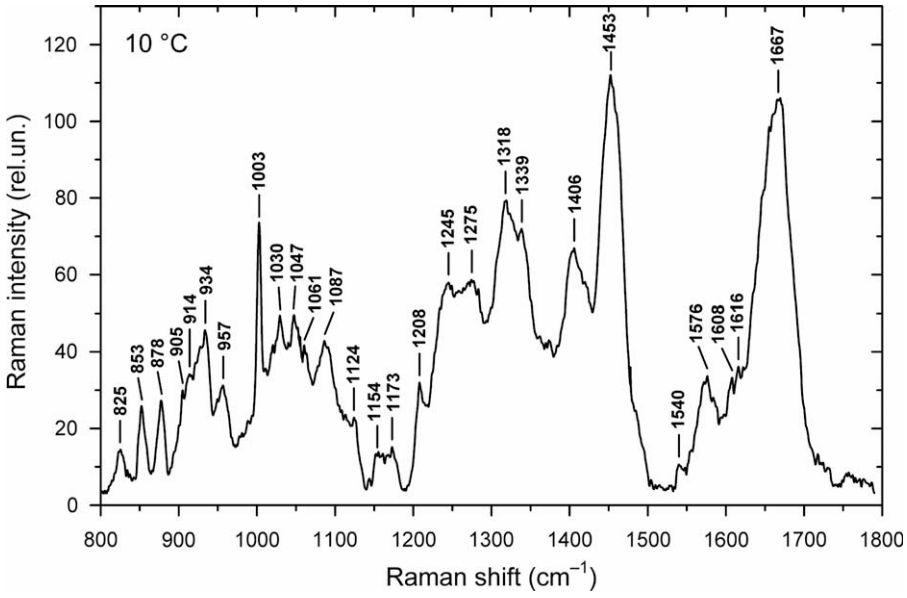

Fig. 4. Raman spectrum of free core-SRF. Peak labels correspond to well resolved bands with precision ±1 cm^{-1}.

core-SRF involves distinctive interactions probably with G bases. Yet a sole core-SRF monomer anchored within SRE^{Gfos} involves changes in the packing of aliphatic side-chains, with a band at 1325 cm^{1}, and in the protein skeleton CC, with a band at 865 cm^{-1} [26]. Probably, strong hydrophobic interactions linked to a water molecule release prevent the polymerization of core-SRF on the oligonucleotide or the formation of the specific protein dimer. Previous fluorescence quenching of core-SRF Tyr residues by SRE^{fos} was static. However, one should note that none of the three Tyr residues of core-SRF is preferentially quenched on SRE^{fos} binding [4]. Thus, the net weakening of H-bonds and the increase in water molecules exposure upon SRE^{fos} binding does not exclude any of the three Tyr residues. Whereas, the accessible fraction of tyrosine emitters affected by SRE^{Gfos} and SRE^{GGfos} fluorescence

quenching decreases with respect to SRE^{fos} excluding some tyrosine fraction from quenching. Thus, the binding interactions of SRE^{fos} with core-SRF involve perturbations evenly distributed on the three Tyr residues, due to a slackening of structural constraints. Moreover, the line broadening of both Tyr doublet components, in average, reflects a wide distribution of the intensity ratio values, hence of a wide distribution of local structural and environmental heterogeneities linked to H-bonds weakening and water molecule exposure.

Conclusion

Analysis of the available crystal structures reveals that the principal DNA feature recognized by core-SRF is the intrinsic and induced conformational properties of DNA [6]. SRE^{fos} conformer interconversion dynamics is decisive for the mutual adjustment of binding partners and the specific core-SRF dimer assembly on SRE^{fos} only reduces their flexibility [12]. The heterogeneities in the core-SRF–SRE^{fos} complex i.e. the polymorphism of the (A/T) domain of the CArG box and the wide distribution of the Tyr intensity doublet ratio, show that the two partners explore a range of various conformations. These heterogeneities originate in the continuous strain variations produced by the conformer interconversion dynamics of SRE^{fos} ensconced in the core-SRF moiety.

In the specific complex, the conversion of SRE^{fos} from a bent form to a linear one does not arise with a release of water molecules of the (A/T) domain like in non-specific complexes. Moreover, the hydration of Tyr residues increases. Thus, water molecules play a crucial role holding the scale of the electrostatic and/or hydrophobic interactions. The specific complex, in solution, is not characterized by a stable bending of SRE, but rather by an electrostatic network deeply linked onto the assembling of a core-SRF dimer on the SRE^{fos} [27]. In this way, the crystallized complexes with a core-SRF homodimer bound to a CArG box are a part of the specific structural distribution allowed to both partners and evidenced in solution.

A particular charge repartition distributed on both core-SRF subunits and SRE moieties is the determining factor of the stability of the assembly of core-SRF homodimer on the oligonucleotide target. It permits the variability of local conformations and generates the specificity of the complex. A broader selection in the recognition of functional CArG boxes by core-SRF is allowed by these distributions of conformations [28].

Acknowledgments

This work was partly supported by the Czech Ministry of Education (project MSM 0021620835). Alberto Mezzetti thanks Fondazione Donegani (Rome) for financial support.

Appendix A. Supplementary data

Supplementary data associated with this article can be found, in the online version, at doi:10.1016/j.bbrc.2009.11.032.

References

[1] T. Gustafson, T. Miwa, L. Boxer, L. Kedes, Interaction of nuclear proteins with muscle-specific regulatory sequences of the human cardiac α-actin promoter, Mol. Cell. Biol. 8 (1988) 4110–4119.
[2] F. Galvagni, M. Lestingi, E. Cartocci, S. Oliviero, Serum response factor and protein- mediated DNA bending contribute to transcription of the dystrophin muscle-specific promoter, Mol. Cell. Biol. 17 (1997) 1731–1743.
[3] A. Parlakian, D. Tuil, G. Hamard, et al., Targeted inactivation of serum response factor in the developing heart results in myocardial defects and embryonic lethality, Mol. Cell. Biol. 24 (2004) 5281–5289.
[4] A. Huet, A. Parlakian, M.-C. Arnaud, et al., Mechanism of binding of serum response factor to serum response element, FEBS J. 272 (2005) 3105–3119.
[5] H. Schröter, C.G. Mueller, K. Meese, A. Nordheim, Synergism in ternary complex formation between the dimeric glycoprotein p67SRF, polypeptide p62TCF and the c-fos serum response element, EMBO J. 9 (1990) 1123–1130.
[6] L. Pellegrini, S. Tan, T.J. Richmond, Structure of serum response factor core bound to DNA, Nature 376 (1995) 490–498.
[7] Y. Mo, W. Ho, K. Johnston, R. Marmorstein, Crystal structure of a ternary SAP-1/SRF/c-fos SRE DNA complex, J. Mol. Biol. 314 (2001) 495–506.
[8] T.A. Gustafson, A. Taylor, L. Kedes, DNA bending is induced by a transcription factor that interacts with the human c-Fos and α-actin promoters, Proc. Natl. Acad. Sci. USA 86 (1989) 2162–2166.
[9] A.G. West, P. Shore, A.D. Sharrocks, DNA binding by MADS-box transcription factors: a molecular mechanism for differential DNA bending, Mol. Cell. Biol. 17 (1997) 2876–2887.
[10] R.R. Koepsel, S.A. Khan, Static and initiator protein-enhanced bending of DNA at a replication origin, Science 233 (1986) 1316–1318.
[11] M.R. Gartenberg, D.M. Crothers, DNA sequence determinants of CAP-induced bending and protein binding affinity, Nature 333 (1988) 824–829.
[12] J. Stepanek, M. Vincent, P.-Y. Turpin, et al., C → G base mutations in the CArG box of c-fos serum response element alter its bending flexibility. Consequences for core-SRF recognition, FEBS J. 274 (2007) 2333–2348.
[13] R. Treisman, Identification of a protein-binding site that mediates transcriptional response of the c-*fos* gene to serum factors, Cell 46 (1986) 567–574.
[14] R.W. Williams, Protein secondary structure analysis using Raman amide I and amide III spectra, Methods Enzymol. 130 (1986) 311–331.
[15] M. Berjot, J. Marx, A.J. Alix, Determination of the secondary structure of proteins from the Raman amide I band: the reference intensity profiles method, J. Raman Spectrosc. 18 (1987) 289–300.
[16] V. Kopecký Jr., R. Ettrich, K. Hofbauerová, V. Baumruk, Vibrational spectroscopy and computer modeling of proteins: solving structure of α_1-acid glycoprotein, Int. J. Spectrosc. 18 (2004) 323–330.
[17] L. Movileanu, J.M. Benevides, G.J. Thomas Jr., Temperature dependence of the Raman spectrum of DNA. II. Raman signatures of premelting and melting transitions of poly(dA).poly(dT) and comparison with poly(dA–dT).poly(dA–dT), Biopolymers 63 (2002) 181–194.
[18] J.M. Benevides, S.A. Overman, G.J. Thomas Jr., Raman, polarized Raman and ultraviolet resonance Raman spectroscopy of nucleic acids and their complexes, J. Raman Spectrosc. 36 (2005) 279–299.
[19] J.M. Benevides, G.J. Thomas Jr., Local conformational changes induced in B-DNA by ethidium intercalation, Biochemistry 44 (2005) 2993–2999.
[20] C. Krafft, J.M. Benevides, G.J. Thomas Jr., Secondary structure polymorphism in *oxytricha nova* telomeric DNA, Nucleic Acids Res. 30 (2002) 3981–3991.
[21] J.M. Benevides, M.A. Weiss, G.J. Thomas Jr., Design of the helix-turn-helix motif: nonlocal effects of quaternary structure in DNA recognition investigated by laser Raman spectroscopy, Biochemistry 30 (1991) 4381–4388.
[22] M.E. El Hassan, C.R. Calladine, Conformational characteristics of DNA: empirical classifications and a hypothesis for the conformational behaviour of dinucleotide steps, Philos. Trans. R. Soc. Lond. A 355 (1997) 43–100.
[23] G.J. Thomas Jr., Y. Li, M.T. Fuller, J. King, Structural studies of P22 phage, precursor particules, and proteins by laser Raman spectroscopy, Biochemistry 21 (1982) 3866–3878.
[24] L. Laporte, J. Stultz, G.J. Thomas Jr., Solution conformations and interactions of α and β subunits of the *Oxytricha nova* telomere binding protein: investigation by Raman spectroscopy, Biochemistry 36 (1997) 8053–8059.
[25] M.N. Siamwiza, R.C. Lord, M.C. Chen, et al., Interpretation of the doublet at 850 and 830 cm^{-1} in the Raman spectra of tyrosyl residues in proteins and certain model compounds, Biochemistry 14 (1975) 4870–4876.
[26] S.A. Overman, G.J. Thomas Jr., Raman markers of nonaromatic side chains in an α-helix assembly: Ala, Asp, Glu, Gly, Ile, Leu, Lys, Ser, and Val residues of phage *fd* subunits, Biochemistry 38 (1999) 4018–4027.
[27] K. Huang, J.M. Louis, L. Donaldson, et al., Solution structure of the MEF2A-DNA complex: structural basis for the modulation of DNA bending and specificity by MADS-box transcription factors, EMBO J. 19 (2000) 2615–2628.
[28] H.Y. Winter, S.J. Marriott, Human T-cell leukemia virus type 1 tax enhances serum response factor DNA binding and alters site selection, J. Virol. 81 (2007) 6089–6098.